Frontiers of Environmental Science & Engineering
2025, 19(6): 83 https://doi.org/10.1007/s11783-025-2003-x

RESEARCH ARTICLE

Risks and mechanistic insights into arsenic-enhanced iodination of bisphenol F in *Brassica chinensis* L.

Kai Zheng[1], Tian Gao[1], Ke Li[1], Yina Guan[1], Shaoyang Hu[1], Yujiang Li[1], Chunguang Liu ✉ [1,2,3,4], Bing Yan[1]

1. School of Environmental Science and Engineering, Shandong Key Laboratory of Environmental Processes and Health, Shandong University, Qingdao 266237, China
2. Laboratory of Marine Ecological Environment in Universities of Shandong, Shandong University, Qingdao 266237, China
3. Qingdao Key Laboratory of Marine Pollutant Prevention, Shandong University, Qingdao 266237, China
4. Shandong Kenli Petrochemical Group Co., Ltd., Dongying 257000, China

HIGHLIGHTS

- BPF iodide products (I-BPF) in *Brassica chinensis* L. rise after As(V) exposure.
- The types and quantities of more toxic I-BPF increase with As(V) exposure level.
- As(V) improves ROS (H_2O_2, •OH) yield, POD activity, which oxidize I^- to RIS.
- Transcriptomics analysis validates that As(V) enhances RIS production in plant.
- More toxic I-BPF are first confirmed and identified in *Brassica chinensis* L.

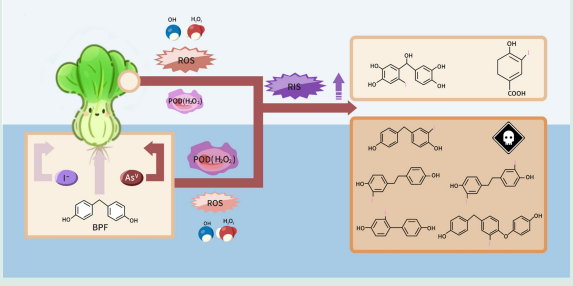

ABSTRACT: Arsenic (As) contamination in vegetables poses significant ecological and health risks, raising substantial public concern. While arsenic accumulation and transformation have been studied, the *in-situ* iodination effects and mechanisms under co-contamination with arsenic and phenolic pollutants (e.g., bisphenol F) remain unclear. This study addresses this gap by exposing *Brassica chinensis* L. to hydroponic solutions containing sodium hydrogen arsenate heptahydrate (As(V)) at concentrations of 0–100 μmol/L, BPF at 3 mg/L, and iodide ions at 40 μmol/L under environmentally relevant conditions. Results demonstrate that As(V) enhances the iodination of BPF by increasing levels of reactive oxygen species (H_2O_2 and •OH) and elevating peroxidase (POD) activity, as confirmed by transcriptomic analysis. As the concentration of As(V) increased from 0 to 100 μmol/L, the diversity and concentration of iodinated BPF products in the roots exhibited a dose-dependent increase, while the variety of iodinated products in the leaves also showed a corresponding rise. Gaussian calculations and mass spectrometry identified the specific substitution sites and the number of iodide atoms incorporated into BPF molecules. By combining toxicity predictions of iodinated BPF using the Toxicity Estimation Software Tool (T·E·S·T) and the Ecological Structure-Activity Relationships (ECOSAR) model with

✉ Corresponding author. E-mail: chunguangliu2013@sdu.edu.cn
Article history: Received 19 February 2025, Revised 2 April 2025, Accepted 3 April 2025, Available online 24 April 2025

measurements of HepG2 cell viability and lactate dehydrogenase (LDH) activity in the cell culture medium, it was found that the toxicity of iodinated BPF products in plants increased following the addition of As(V). This study highlights the combined risks of arsenic and bisphenol contamination, revealing arsenic's role in enhancing bisphenol iodination and toxicity in plants.

KEYWORDS: As(V) pollution, Iodination of bisphenol F, Vegetable safety, Toxicity analysis

1 Introduction

Arsenic (As) contamination is a growing global concern due to its severe ecological and health impacts (Appelo et al., 2002). In China, groundwater arsenic levels can reach up to 12 mg/L (Kim et al., 2012). The long-term irrigation with contaminated water has increased soil arsenic concentrations, in Bangladesh, where levels rose from 57 to 83 mg/kg (Alam and Sattar, 2000; Panda et al., 2010). Due to its stability under aerobic conditions, As(V) is more commonly found in agricultural environments where crops are cultivated (Wang et al., 2021b; Cai et al., 2022). This persistent use of contaminated water for crop irrigation has led to significant arsenic accumulation in grains and vegetables (Bednar et al., 2002; Tripathi et al., 2007; Zhu et al., 2008). When plants absorb inorganic arsenic, reactive oxygen species (ROS) such as hydrogen peroxide (H_2O_2) and hydroxyl radicals (•OH) are generated, causing oxidative stress (Hartley-Whitaker et al., 2001). Consuming arsenic-contaminated crops is linked to various health issues, including metabolic disorders, kidney disease, cardiovascular conditions, cancer, and maternal-fetal complications (Khan et al., 2021).

Apart from arsenic, the presence of emerging phenolic contaminants in the consumable portions of vegetables has raised growing health concerns (Matschullat, 2000; Meharg and Hartley-Whitaker, 2002; Huang et al., 2019; Yao et al., 2020; Kovačič et al., 2023). However, the effects of arsenic on these emerging pollutants, particularly under conditions of ubiquitous iodine ion (I^-) presence, remain poorly understood. Bisphenol pollutants, such as bisphenol F (BPF), have garnered significant attention due to their widespread use and high bioaccumulation potential in plants (Dodgen et al., 2013), BPF has been identified in a range of crops and fruits, with concentrations ranging from 3.3 to 4.6 mg/kg in *C. viridevar.* and up to 7.2 mg/kg in *Bracteatum G. faberi* (Lu et al., 2013; Huang et al., 2019). Compared to bisphenol A (BPA), BPF exhibits more pronounced adverse effects on spring rapeseed yield, showing significant inhibition in soil contaminated with 5 mg/kg of BPF (Zaborowska et al., 2023). Despite being a BPA substitute, BPF still poses significant reproductive and genetic toxicity risks, evidenced by a high detection rate of 66.5% in the urine of both adults and children (Lehmler et al., 2018; Ding et al., 2022).

Phenolic pollutants like BPF can react with reactive halogens in the presence of free radicals to form more toxic organic pollutants. Iodine, ubiquitous in the environment, primarily exists as an inorganic iodine species (I^- and IO_3^-) (Hetzel, 2009). In soils, iodine concentrations range from 0.1 to 660 mg/kg, with a median value of 3 mg/kg (Johnson, 2003; Smyth and Johnson, 2011). Natural surface water iodine concentrations vary from 0.004 to 0.787 μmol/L, with some drinking water sources containing up to 32.417 μmol/L (Tang et al., 2013). Groundwater generally exhibits higher iodine concentrations, reaching up to 114.173 μmol/L in Denmark, 267.716 μmol/L in Japan, and 48.000 μmol/L in Chile. In China, groundwater iodine levels are notably high, with concentrations of 36.228 μmol/L detected in Shandong and peaking at 222.519 μmol/L in the Guanzhong Basin (Duan et al., 2016; Wang et al., 2021c).

Iodide (I^-) readily transforms into reactive iodine species (RIS) such as hypoiodous acid (HIO), iodine radicals ($I^•$), iodide ions (I_2^-), and triiodide ions (I_3^-) through various pathways involving reactive oxygen species (ROS) and enzymatic reactions (Buxton et al., 1988; Milenković and Stanisavljev, 2012; Chen et al., 2021; Mackeown et al., 2022; Wang et al., 2022a). RIS exhibits selective reactivity, primarily targeting phenolic compounds like BPF and α-methyl carbonyl compounds such as acetaldehyde and acetone (Bichsel and Von Gunten, 2000; Ding and Zhang, 2009; Li et al., 2018). The iodine-containing byproducts formed in these reactions are generally more toxic than other halogenated byproducts. Specifically, iodinated disinfection byproducts (I-DBPs) demonstrate more potent cytotoxicity and genotoxicity compared to their brominated or chlorinated counterparts (Wagner and Plewa, 2017; Dong et al., 2019; Gonsioroski et al., 2020). Furthermore, arsenic and iodide co-contamination of groundwater is common in many

regions (Pi et al., 2015; Wang et al., 2018). Arsenic stress in plants induces a burst of ROS (Begum et al., 2016; Tiwari and Sarangi, 2017). And a significant increase in the activity of various antioxidant enzymes (Mishra et al., 2011; Vezza et al., 2022). These biochemical changes can influence the transformation of I^- into RIS within plants, thereby affecting the iodination of phenolic pollutants.

This study employs arsenate (As(V)) as a representative metalloid pollutant and BPF as a representative phenolic pollutant to investigate 1) the effects of As(V) on the iodination of BPF in *Brassica chinensis* L. with I^- and 2) the iodination pathways, identification of iodinated products, and evaluation of their ecological risks.

2 Materials and methods

2.1 Chemicals

BPF (≥ 98%), salicylhydroxamic acid (SHAM, ≥ 98%), methyl alcohol (≥ 99%), diphenyliodonium chloride (DPI, ≥ 98%), 4-Hydroxy Tempo (≥ 98%), and chromatography-grade acetonitrile (≥99%) were obtained from Macklin (Shanghai, China). $Na_2HAsO_4{\cdot}7H_2O$ (≥ 98%) and Dimethyl-*p*-phenylenediamine (DPD, ≥ 98%) were purchased from Aladdin (Shanghai, China). Potassium iodide (≥ 99%), 30% hydrogen peroxide (≥ 30%), disodium hydrogen phosphate (≥ 99%), and sodium dihydrogen phosphate (≥ 99%) were sourced from Sinopharm Chemical Reagent Co., Ltd., Shanghai, China. Sample details are available in Table S1 of the supplementary material.

2.2 Cultivation and management of *Brassica chinensis* L.

The seeds of *Brassica chinensis* L. were sterilized by immersing them in 10% H_2O_2 for 10 min, followed by soaking at 30 °C for 12 h. They were then germinated in the dark at 26 °C for two days. After germination, the seedlings were transferred to a hydroponic system containing 100% Hoagland nutrient solution under sterile conditions and cultivated in a sterile growth chamber. The plants were maintained under an 18-h light/6-h dark photoperiod at 26 °C/24 °C (Dong et al., 2023). The nutrient solution was renewed every two days to prevent bacterial growth, and after two weeks, it was replaced with a 25% diluted solution. All procedures, including nutrient solution preparation and seedling transfer, were conducted aseptically to ensure a sterile environment. The specific operation details and cultivation parameters are provided in the supplementary material Text S1.

2.3 Experimental treatment of *Brassica chinensis* L.

The experiment used *Brassica chinensis* L. with stable growth for 45 d, exposed to a mixed nutrient solution containing I^-, BPF, and different As(V) levels. Three groups were established by adding a peroxidase inhibitor (SHAM), NADPH oxidase inhibitor (DPI), and hydrogen peroxide scavenger (4-Hydroxy-Tempo), with samples collected for analysis after 5 d. The specific details of the exposure experiment and the selection of inhibitor concentrations are referenced in the supplementary material Text S2.

2.4 Assay methods

2.4.1 Homogenization of *Brassica chinensis* L. tissue samples

Plant root or leaf tissues were quickly frozen in liquid nitrogen and homogenized in 0.1 mol/L phosphate-buffered saline (pH 7.2, 4 °C) using a SCIENTZ-48LT grinder at a ratio of 0.1 g tissue per 1 mL buffer. The homogenate was centrifuged at 11500 g for 15 min at 4 °C (Shanghai Flying Pigeon, TGL-16G, China), and the supernatant was collected for further analysis.

2.4.2 Determination of reactive iodine species

Brassica chinensis L. root and leaf samples (0.5 g) were homogenized, followed by centrifugation to collect the supernatant. The RIS (I_2, I_3^-, and HIO) in the tissue samples were measured in this study using the DPD (*N*,*N*-diethyl-*p*-phenylenediamine) method. A 5 mL sample was sequentially mixed with 0.5 mL of 0.5 mol/L phosphate buffer (pH 6.0) and 0.5 mL of standard DPD solution. Optical measurements were performed using a UV spectrophotometer (SHIMADZU, UV-2600, Japan), completed rapidly within 20 s. This method has been widely used for detecting RIS (Brion and Silverstein, 1999; Chen et al., 2021). The total amount of RIS (I_2, I_3^-, and HIO) was quantified using the DPD method by measuring the formation of $DPD^{\bullet+}$, which exhibits strong absorbance at 551 nm (ε = 21000 $M^{-1}{\cdot}cm^{-1}$). Due to the complexity of the tissue sample, the presence of H_2O_2 in it can be rapidly oxidized by peroxidases, leading to the accuracy of its absorbance at 551 nm, and the presence of other organic substances, such as

chlorophyll, may also affect the accuracy of absorbance at 551 nm. It is, therefore necessary to pre-treat the grinding solution of the tissue samples before measurement to ensure that the solution being measured is inorganic. In Text S3 and Fig. S1, we give the specific operation of the pretreatment step. We conducted preliminary pre-tests on the grinding solution of untreated *Brassica chinensis* L. roots and leaves post-pretreatment to validate the effectiveness of the pretreatment process. Its experimental results showed that the pretreatment was effective in eliminating the interference of organic substances (chlorophyll, etc.) and substances such as peroxidase, and that its color development and absorbance were almost the same as those of deionized water (Figs. S2 and S3), which also ensured the accuracy of the subsequent RIS measurement by the DPD method.

2.4.3 Determination of hydrogen peroxide content, POD activity, and SOD activity, as well as the ability to produce $O_2^{\bullet-}$ and •OH

Fresh *Brassica chinensis* L. roots and leaves (0.1 g) were ground into a homogenate, and the supernatant was collected after centrifugation. The grinding solution was prepared according to the instructions provided with the Nanjing jiancheng reagent kit. The levels of H_2O_2, hydroxyl radicals (•OH), superoxide anions ($O_2^{\bullet-}$), and the activities of peroxidase (POD) and superoxide dismutase (SOD) were assessed using the kit's protocol.

2.4.4 Analysis of transformed products and assessment of BPF levels

Brassica chinensis L. root and leaf samples (0.5 g) were homogenized, and the supernatant was collected after centrifugation. The extract underwent solid-phase extraction (SPE), was eluted with methanol, concentrated to 1 mL, and filtered through a 0.22 μm membrane. BPF transformation products and pathways were analyzed via LC-MS/MS (TSQ Quantum Access MAX, Thermo Scientific, USA) with negative electrospray ionization (ESI). The separation utilized a reverse-phase C18 column (50 mm × 2 mm, 4 μm) with modified HPLC conditions as described by Yu et al. (2020) and Guo et al. (2021). The UV detection was conducted at a wavelength of 243 nm using a mobile phase composed of acetonitrile and water in a 60:40 ratio, with a flow rate of 0.5 mL/min and an injection volume of 20 μL. The mass spectrometry setup featured a 3000 V capillary voltage, 8.0 eV capillary energy, 550.0 Vpp collision cell RF, and an MS scan range of 60–500 m/z. The content of BPF in fresh root and leaf samples was quantified using HPLC under the same pretreatment and chromatographic conditions as LC-MS/MS.

2.5 Transcriptomics and q-PCR analysis

Brassica chinensis L. was subjected to various treatments for 5 d, after which 0.2 g samples of root or leaf tissues were collected, thoroughly washed with deionized water, flash-frozen in liquid nitrogen, and stored at −80 °C. RNA was isolated from tissue samples, and its concentration and purity were assessed with a spectrophotometer (NanoDrop 2000, Thermo Scientific, USA). RNA integrity was evaluated using agarose gel electrophoresis, and the RNA integrity number (RIN) was measured with a bioanalyzer (Agilent 2100, Agilent, USA). mRNA was extracted from total RNA using magnetic beads with Oligo (dT), which binds to the polyA tail of mRNA via A-T base pairing. Sequencing was performed on the Illumina platform (Shanghai Meiji Biotechnology, China) targeting short-read sequences. A fragmentation buffer was introduced to randomly cleave the mRNA into ~300 bp fragments, which were then isolated via magnetic bead screening. Double-stranded cDNA was synthesized by first generating first-strand cDNA from mRNA using reverse transcriptase and random hexamer primers, followed by second-strand synthesis. The double-stranded cDNA's sticky ends were converted to blunt ends using End Repair Mix, followed by the addition of an 'A' base to the 3' ends to facilitate ligation with Y-shaped adapters. Sequencing was performed on the Illumina platform, and differentially expressed genes shared between roots and leaves were selected for q-PCR analysis. Real-time quantitative PCR was conducted using the Applied Biosystems StepOne™ Real-Time PCR system, with primer sequences detailed in Supplementary Table S2. Reference genomes were from Ensembl Genomes.

2.6 Toxicity assessment

The ecological toxicity variations of BPF and its iodinated products were comprehensively predicted using two software tools: Ecological Structure Activity Relationships (ECOSAR, version 2.2) and the Toxicity Estimation Software Tool (T·E·S·T, version 5.1.2) (Chen et al., 2018; Svedberg et al., 2023; Xu et al., 2024). Both tools utilize advanced QSAR models to predict compound toxicity from molecular structures. These tools have been internationally recognized and validated for predictions (Claeys et al., 2013; Khan

et al., 2019). The ECOSAR model assessed the acute and chronic toxicity of BPF and its iodinated derivatives on three aquatic species: fish, daphnia, and green algae. The T·E·S·T software evaluated the acute toxicity of BPF and its iodinated derivatives on four organisms: fathead minnow (Pimephales promelas), Daphnia magna, and Tetrahymena pyriformis. Toxicity parameters encompassed LC_{50} (median lethal concentration), IGC_{50} (50% inhibitory growth concentration), developmental toxicity, and mutagenicity.

2.7 Cytotoxicity analysis

HepG2 cells were obtained from the China Cell Bank. Detailed procedures for cell culture and passaging are outlined in Text S4 (Hercog et al., 2019; Wang et al., 2021a; Yu and Liu, 2023). A slurry was prepared by homogenizing 0.1 g of fresh plant roots and leaves, followed by centrifugation. The supernatant was then collected and filtered through a 0.22 μm membrane to eliminate macromolecular proteins. To investigate the toxicity of organic compounds in the plant samples, the supernatant was passed through an SPE solid-phase extraction column, eluted with methanol, and then used to expose HepG2 cells. HepG2 cells were treated with a 0.5% concentration of both the organic extract solution and the self-prepared BPF solution for 48 h (Fig. S4). This concentration ensured uniformity and minimized the potential toxicity of methanol as a solvent (Nguyen et al., 2020). The BPF concentrations in the prepared solutions matched those found in 0.1 g of homogenized leaf or root tissue per 1 mL of grinding buffer for each treatment group. The Nanjing Jiancheng Bioengineering Institute assay kits were used to measure cell viability (CCK-8 assay) and lactate dehydrogenase (LDH) activity in the cell culture medium.

2.8 Data analysis

Each experimental treatment was performed three times, and the outcomes were presented as the average ± standard deviation (SD). Statistical analysis was conducted using SPSS 25.0, with one-way ANOVA applied to assess significance at $p < 0.05$. Post-hoc tests were conducted using LSD, Tukey's b, and Waller-Duncan methods. *t*-tests with Studentized range distributions were used to evaluate pairwise comparisons of group means, and multiple comparisons were also conducted using *t*-statistics. Moreover, Bayesian techniques were utilized for further statistical analysis (Gu et al., 2020; Kundu et al., 2024). Gaussian 09W calculates $2FED^2_{HOMO}$ per carbon before iodine electrophilic substitution.

3 Results and discussion

3.1 As(V) exposure enhances the iodination of BPF in *Brassica chinensis* L.

3.1.1 The iodinated products of BPF in *Brassica chinensis* L.

Figures 1(a)–1(c) and 1(d)–1(f) display the full scan mass spectra of BPF transformation products in the roots and leaves of cabbage exposed to 0, 25, and 100 μmol/L As(V), with different iodinated products highlighted in different colored boxes (the corresponding EIC plots are shown in the supporting information, Fig. S5). The identification of these iodine-containing transformation products (namely TP1–TP7) is based on the characteristic ion m/z 127 found in the secondary mass spectrometry results (Figs. S6–S12), and the m/z values of iodine-containing ions detected in the samples are listed. The structures of the substances were inferred based on the secondary mass spectrometry data. For example, TP5 is inferred to be a substance containing two iodine because molecular ion peaks are observed at m/z 211 and 210 which differ from the precursor ion by 254 and 255 Da, indicating the loss of two iodine atoms or one iodine and one HI, and, molecular ion peaks are found at m/z 127 and 128, which further confirms that it contains two iodine. At the same time, it was also observed that the molecular ion peak containing m/z was 232, which was 233 different from the precursor ion, that is, C_7H_6OI, which was believed to be dropped by the breakdown of the carbon bridge bond formed by two carbons in TP5, and the molecular ion peak with a difference of 127 m/z was found to be 105 with the molecular ion peak of 232, which proved that the molecular ion peak of 232 also contained iodine. These data support our description of the structure of TP5 (Fig. S10). Due to the lack of standards, further structural confirmation could not be performed, so theoretical calculations were used to determine the specific positions of iodine substitution. The carbon atoms that are most likely to be electrophilically substituted by BPF, TP2-1, TP3-1, TP4-1, TP4, TP6-1, and TP7-1 are shown in Fig. S13. The corresponding values are detailed in Table S3.

3.1.2 As(V) increased the type and content of iodinated products in *Brassica chinensis* L.

As shown in Fig. 2(a), the number of iodinated products

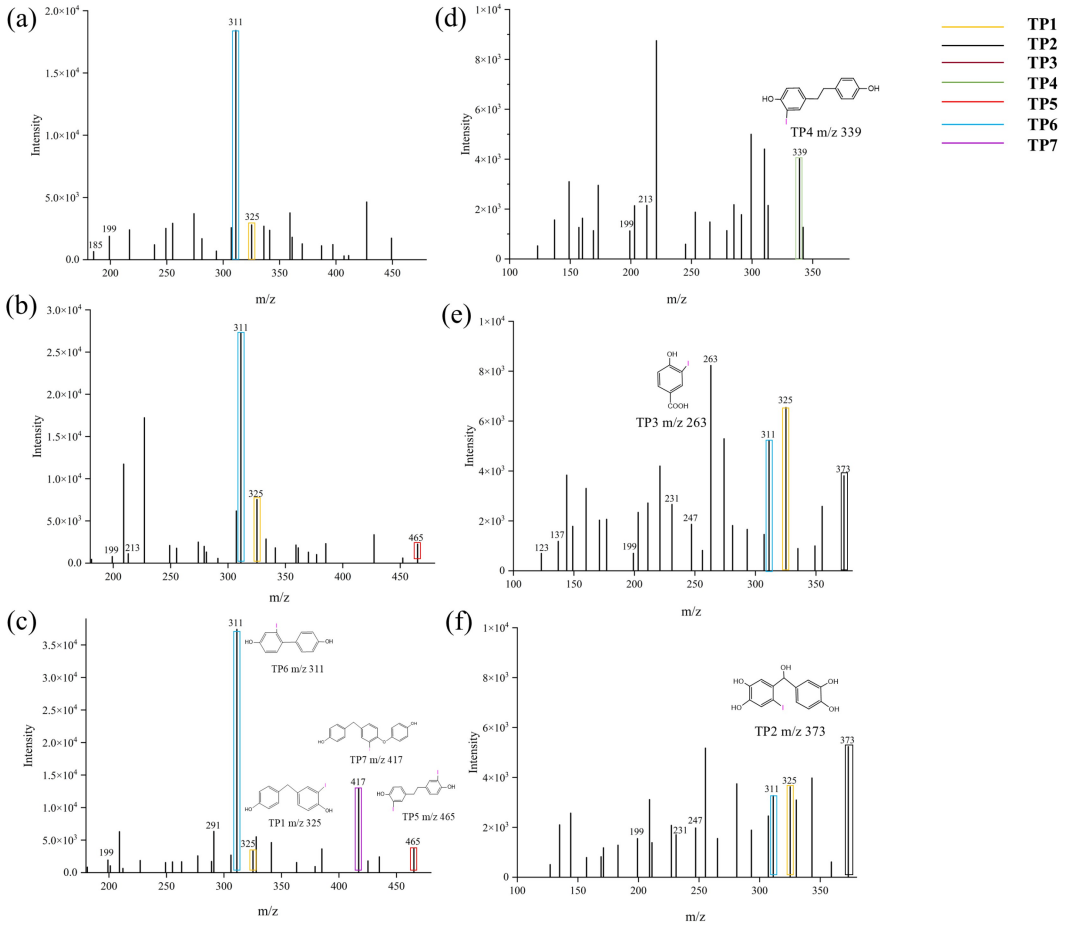

Fig. 1 Peak intensities of BPF transformation products in roots (a–c, 0, 25, 100 μmol/L) and leaves (d–f, 0 , 25, 100 μmol/L) identified by LC-MS/MS at different concentrations of As(V).

in roots increased with rising As(V) concentrations. Notably, the peak areas of newly formed TP5 and TP6 in roots also increased with higher As(V) concentrations, and at 100 μmol/L As(V), a root-specific iodinated product, TP7, was observed. Similarly, in the leaves, the types of iodinated products increased after adding As(V), and the peak area of iodinated product TP2 increased with the addition of As(V) concentration, reaching its maximum at 100 μmol/L As(V) (Fig. 2(b)).

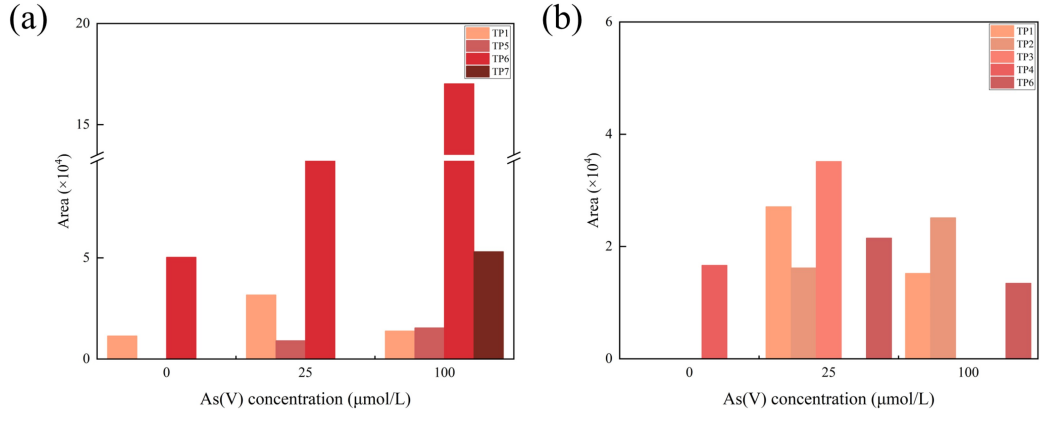

Fig. 2 Peak areas of BPF iodide products in (a) roots and (b) leaves of *Brassica chinensis* L. under different As(V) (0, 25, 100 μmol/L) treatments. C_{BPF} = 3 mg/L, C_{I^-} = 40 μmol/L.

Combined with the results of Figs. 1 and 2, the addition of As(V) increases the type and number of iodide products in the roots, while the diversity of iodide products in the leaves enriches the diversity of iodide products, although the iodine products formed in the roots and leaves are not the same. Thus, the addition of As(V) enhances the iodination of BPF.

3.1.3 The generation pathway of iodinated products during the BPF transformation in *Brassica chinensis* L.

Based on the m/z values in the primary mass spectra and a review of relevant literature, the iodinated products of BPF may be formed through the following three generation pathways: (I) BPF can be directly electrophilically replaced by RIS to form the iodinated product TP1. (II) BPF may react with •OH radicals to initially produce intermediates A1-1 or A1-2 (m/z 231), which then convert into TP2-1 (m/z 247) before undergoing substitution by RIS to form the iodinated product TP2. This hydroxylation process is well-documented and has been studied in previous research (Morales-Roque et al., 2009; Porcar-Santos et al., 2022). (III) Reactive species within plant tissues may directly oxidize to attack BPF, resulting in β bond cleavage and the formation of *p*-hydroxybenzyl alcohol (A2, m/z 123) and phenol (A3). As phenolic compounds, A2 and A3 may undergo chemical oxidation or react with peroxidase (in H_2O_2) to form phenoxy radicals. These phenoxy radicals can then be coupled at different locations to produce dimers or oligomers (Henriksen et al., 1999; Laurenti et al., 2003; Yang et al., 2020; Jia et al., 2022; Liu et al., 2022). A2 may undergo self-coupling to form TP4-1 (m/z 213), which can then be substituted by reactive iodine species (RIS) to produce TP4. The diiodinated product TP5 may arise through two pathways: further electrophilic substitution of TP4 by RIS or direct electrophilic substitution of TP4-1 by additional RIS. The formation of TP6 is likely initiated by the self-coupling of A3 to form TP6-1, followed by electrophilic substitution with RIS. In addition, A3 may promote TP7 production through two possible pathways: direct coupling to TP1 or conjugation to BPF to form TP7-1, which is then substituted by RIS electrophiles, leading to the formation of TP7 (Fig. 3).

3.2 Iodination mechanisms of BPF with As(V) exposure in *Brassica chinensis* L.

3.2.1 As(V) promotes the iodination of BPF by elevating POD activities in *Brassica chinensis* L.

Numerous studies have shown that As(V)

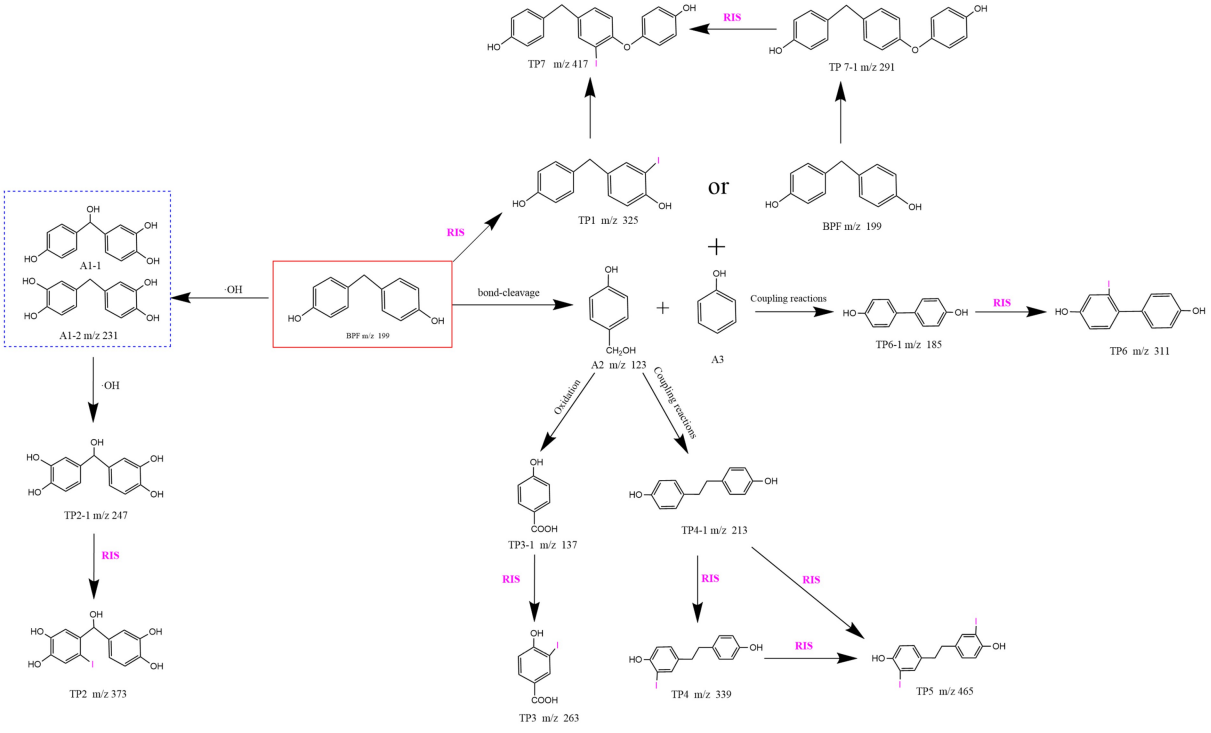

Fig. 3 The generation pathway of internal iodinated products in *Brassica chinensis* L.

contamination can induce changes in the activities of various antioxidant enzymes in plants, including POD, SOD, catalase (CAT), and glutathione S-transferase (GST) (Mascher et al., 2002; Bianucci et al., 2017; Tzean et al., 2024). Without As(V), the POD activity in both roots and leaves did not show significant increases. However, upon the addition of As(V), POD activity in roots and leaves increased with rising As(V) concentrations, with the changes in root POD activity being more pronounced than those in leaves (Fig. 4(a)). Previous studies have demonstrated that Class III peroxidases (POD), such as horseradish peroxidase (HRP), can catalyze the transformation of I^- into RIS (HIO, I_2, I_3^-, etc.) in the presence of H_2O_2, which then react with organic pollutants to produce iodinated products (Table 1, Eqs. (1)–(3)) (Wang et al., 2022a).

The levels of RIS were measured, revealing that after the addition of As(V), RIS in both roots and leaves increased with rising As(V) concentrations, peaking at 100 μmol/L As(V) (Fig. 4(b)). Since previous studies have shown that POD can oxidize I^- to RIS, we infer that As(V) may promote the production of RIS in the roots and leaves of *Brassica chinensis* L. by stimulating the activity of POD. To further confirm this, SHAM, a potent POD inhibitor, was introduced to the group with the highest RIS production. The results showed a reduction of RIS by 36.12% in roots and 13.85% in leaves (Fig. 4(c)). These findings indicate that As(V) likely promotes the conversion of I^- to RIS by enhancing POD activity in the roots and leaves of *Brassica chinensis* L., thereby increasing the iodination of BPF within the plant.

3.2.2 As(V)-induced oxidative stress enhancing the iodination of BPF in *Brassica chinensis* L.

3.2.2.1 The role of hydrogen peroxide

After adding As(V), the H_2O_2 levels in both the roots and leaves increased to varying degrees, reaching a peak at 100 μmol/L As(V) (Fig. 5(a)). Although exposure to BPF alone also caused a slight increase.

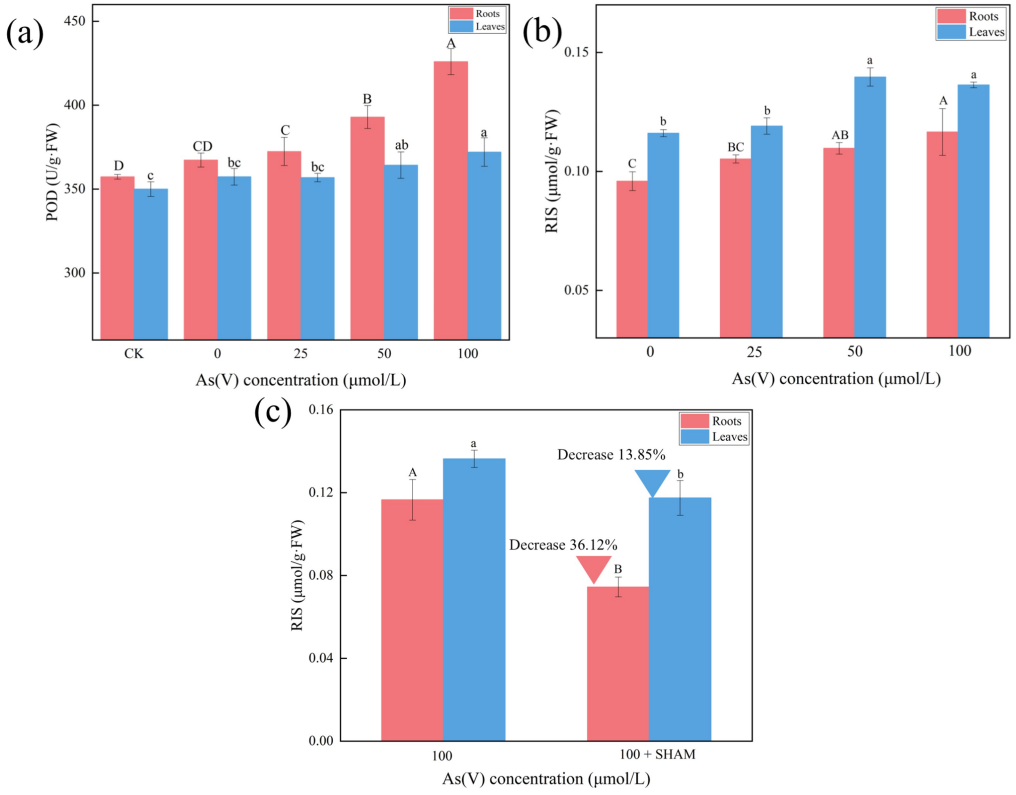

Fig. 4 Changes in (a) POD activity and (b) RIS in roots and leaves of *Brassica chinensis* L. under different As(V) treatments, (c) changes in RIS of roots and leaves after adding POD inhibitor SHAM at As(V) concentration of 100 μmol/L. C_{BPF} = 3 mg/L, C_{I^-} = 40 μmol/L. C_{SHAM} = 150 μmol/L. The letter labeling method was used in the figure to present the results of difference analysis. Groups labeled with different letters indicate statistically significant differences ($p < 0.05$), while groups sharing the same letter indicate no significant differences. In the figure, uppercase letters represent root groups, and lowercase letters represent leaf groups.

Table 1 Summary of equations involving RIS generation

Equation	Serial number
$2I^- \xrightarrow{POD(H_2O_2)} I_2$	Equation (1)
$I_2 + H_2O \rightarrow HIO + H + I^-$	Equation (2)
$I_2 + I^- \rightarrow I_3^-$	Equation (3)
$H_2O_2 + 2I^- + 2H^+ \rightarrow I_2 + 2H_2O$	Equation (4)
$H_2O_2 + I^- + H^+ \rightarrow HIO + H_2O$	Equation (5)
$H_2O_2 + O_2^{\bullet -} \rightarrow \bullet OH + OH^- + O_2$	Equation (6)
$H_2O_2 \xrightarrow{hv/Fenton} \bullet OH + OH^-$	Equation (7)
$\bullet OH + I^- \rightarrow OH^- + I^\bullet$	Equation (8)
$I^\bullet + I^\bullet \rightarrow I_2$	Equation (9)
$I_2 + OH^- \rightarrow HIO + I^-$	Equation (10)
$I^\bullet + I^- \rightarrow I_2^{\bullet -}$	Equation (11)
$I_2^{\bullet -} + I^- \rightarrow I_3^{\bullet -}$	Equation (12)
$2I_2^{\bullet -} \rightarrow I_3^{\bullet -} + I^{\bullet -}$	Equation (13)

H_2O_2 is typically generated through the conversion of $O_2^{\bullet -}$ under the action of superoxide dismutase (SOD) (Quan et al., 2008). After the addition of As(V), the SOD activity and the ability to produce $O_2^{\bullet -}$ in both roots and leaves increased to varying degrees, which explains the elevated H_2O_2 levels in different tissues of *Brassica chinensis* L. after As(V) exposure (Fig. S14). Notably, H_2O_2 levels in leaves were higher than those in roots. This could be attributed to the higher POD activity in roots compared to leaves, leading to the conversion and decomposition of more H_2O_2 in root tissues (Fig. 4(a)). H_2O_2, as the longest-lived ROS (Bhattacharjee, 2005; Quan et al., 2008), possesses sufficient oxidative capacity to convert I^- into RIS (Table 1, Eqs. (2)–(5)) (Chen et al., 2021; Wang et al., 2022a; Xu et al., 2023; Shao et al., 2024). To further verify its role, 4-Hydroxy Tempo, an effective H_2O_2 scavenger (Wang et al., 2022b; Deng et al., 2023), was added to the experimental group with the highest RIS production. This resulted in a 40.73% reduction in RIS levels in roots and a 19.32% reduction in leaves (Fig. 5(b)). Compared to the use of peroxidase inhibitors, the more pronounced suppression of RIS levels may be attributed to 4-Hydroxy Tempo not only eliminating H_2O_2 but also indirectly limiting the POD-mediated pathway for RIS production. These findings suggest that As(V) likely enhances the iodination of BPF in *Brassica chinensis* L. by increasing H_2O_2 levels in roots and leaves, thereby promoting RIS production.

3.2.2.2 The role of hydroxyl groups

As shown in the Fig. 6(a), in the absence of As(V), there was no significant variation in the ability of leaves to produce •OH, while roots showed a slight increase, though not markedly different. After the addition of various concentrations of As(V), the ability to produce •OH increased to varying degrees in leaves, whereas in roots, a significant increase was observed only at a concentration of 100 μmol/L As(V) (Fig. 6(a)).

$O_2^{\bullet -}$, as the initial reactive oxygen species, can be converted into H_2O_2, which can then generate hydroxyl radicals (•OH) through photolysis in the Haber-Weiss reaction and reactions with transition metals (Eqs. (6)

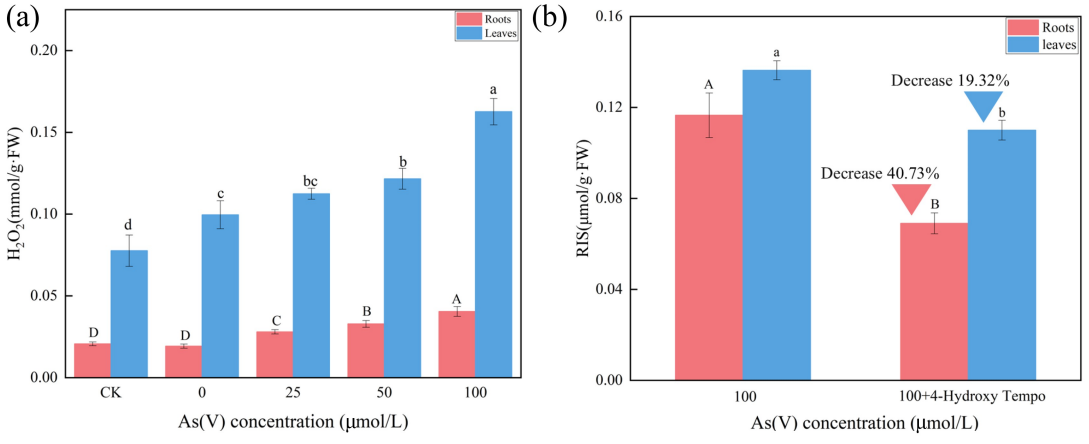

Fig. 5 Changes in H_2O_2 (a) in roots and leaves of *Brassica chinensis* L. under different As(V) conditions (0, 25, 50, 100 μmol/L), (b) the changes in RIS of roots and leaves after adding H_2O_2 scavenger 4-Hydroxy Tempo at an As(V) concentration of 100 μmol/L. C_{BPF} = 3 mg/L, C_{I^-} = 40 μmol/L. $C_{4\text{-Hydroxy Tempo}}$ = 40 μmol/L, C_{DPI} = 15 μmol/L. The letter labeling method was used in the figure to present the results of difference analysis. Groups labeled with different letters indicate statistically significant differences ($p < 0.05$), while groups sharing the same letter indicate no significant differences. In the figure, uppercase letters represent root groups, and lowercase letters represent leaf groups.

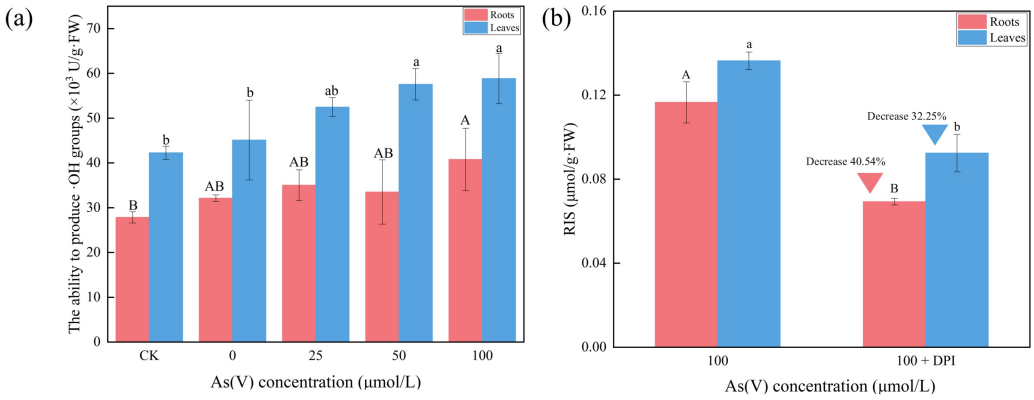

Fig. 6 Changes in hydroxyl generation ability (a) in roots and leaves of *Brassica chinensis* L. under different As(V) conditions (0, 25, 50, 100 μmol/L), the changes in RIS (b) of roots and leaves after adding NADPH oxidase inhibitor at an As(V) concentration of 100 μmol/L. C_{BPF} = 3 mg/L, C_{I^-} = 40 μmol/L. C_{DPI} = 15 μmol/L. The letter labeling method was used in the figure to present the results of difference analysis. Groups labeled with different letters indicate statistically significant differences ($p < 0.05$), while groups sharing the same letter indicate no significant differences. In the figure, uppercase letters represent root groups, and lowercase letters represent leaf groups.

and (7)) (Chen and Schopfer, 1999; Richards et al., 2015). Therefore, it plays a critical role in the formation of •OH. •OH, as the most oxidizing species among ROS, can easily convert I^- into various RIS ($I^•$, $I_2^{•-}$, $I_3^{•-}$, I_2, HIO, I_3^-) (Eqs. (2), (3), (5) and (8)–(13)), however, $O_2^{•-}$ itself cannot directly oxidize I^-. Previous studies have shown that NADPH oxidase is involved in arsenic-induced ROS production in various plants, including peanut (Bianucci et al., 2017), rice (Kushwaha et al., 2019), and tomato (Siddiqui et al., 2024). In plants, NADPH oxidase (respiratory burst oxidase homologs) serves as a major source of $O_2^{•-}$, and its impairment can significantly reduce •OH generation (Renew et al., 2005; Glyan'ko and Ischenko, 2010; Heyno et al., 2011).

Therefore, the effective NADPH oxidase inhibitor DPI was added in the experimental group with the highest RIS production. After the addition of DPI, RIS levels in roots decreased by 40.54%. In comparison, in leaves they decreased by 32.25% (Fig. 6(b)). In leaves, the inhibition rate of RIS production with DPI was further improved compared to that with 4-Hydroxy Tempo, likely due to the additional suppression of •OH-mediated oxidation of I^- to RIS, on top of inhibiting POD and H_2O_2 pathways. However, in roots, the inhibition rate of RIS production with DPI was not further enhanced compared to 4-Hydroxy Tempo. This phenomenon occurs because the increase in •OH production in roots after As(V) exposure is not as significant as in leaves, resulting in a less pronounced contribution of •OH to RIS formation (Fig. 6(a)). These findings suggest that As(V) may enhance the iodination of BPF in *Brassica chinensis* L. by increasing the production of •OH in roots and leaves, which in turn boosts RIS formation.

3.3 Using PCA analysis to conduct a correlation analysis on the mechanism of enhancing *Brassica chinensis* L. BPF iodization by As(V)

Principal component analysis (PCA) has advantages in dimensionality reduction, multicollinearity, revealing global structure, visualization and synthesis of information, and is suitable for high-dimensional data analysis and pattern recognition. However, the Spearman and Pearson correlation is more suitable for analyzing the specific relationship between the two variables, so the PCA analysis was used to explore the relationship between the ability of roots and leaves to produce •OH, H_2O_2 content, POD activity, and RIS changes in the experimental group with different As(V) concentrations. The results indicate that in both roots and leaves, H_2O_2, •OH, and POD were positively correlated with RIS (Fig. 7). In roots, the increase in RIS production with rising As(V) concentrations was more closely related to changes in H_2O_2 content and POD activity, while •OH also showed a positive correlation but appeared to play a less dominant role, aligning with our earlier hypothesis based on the results of adding DPI. H_2O_2 likely plays a critical role in root RIS production due to its dual capacity to directly oxidize I^- into RIS and to serve as a substrate for POD to convert I^- into RIS (Fig. 7(a)). In leaves, POD did not appear to dominate RIS production, while •OH and H_2O_2 were more strongly associated with RIS. This may be due to the lower POD activity in leaves than roots, leaving more H_2O_2 unutilized, indirectly promoting •OH production. Both H_2O_2 and •OH can

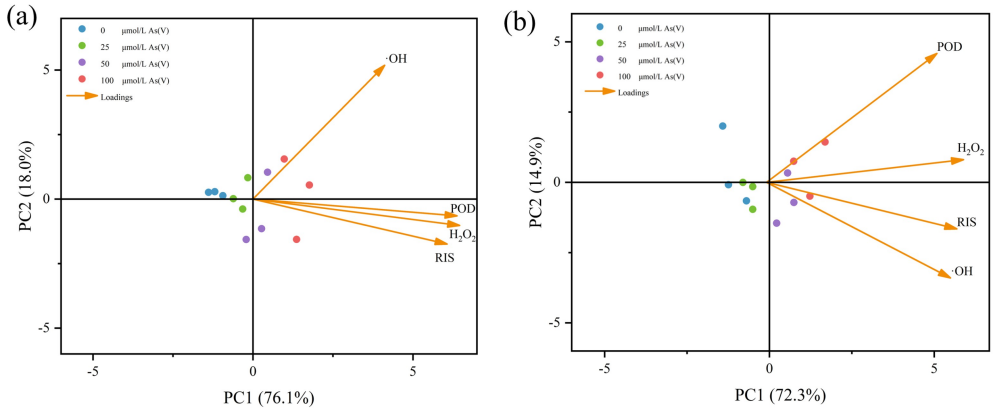

Fig. 7 Different As(V) treatments may affect the PCA analysis of enhanced RIS components in (a) roots and (b) leaves. If the direction of the arrows identified by the different labels is consistent, it indicates a positive correlation, and if the direction is inconsistent, it indicates a negative correlation. The smaller the angle of the arrows with the same direction, the stronger the correlation. The dots in the graph represent different treatment groups, and the more distant the two treatment groups are, the more significant the positive and negative correlation is proved.

independently oxidize I^- into RIS, explaining the formation of the polyhydroxylated iodinated product TP2 in leaves, which was not observed in roots. Compared to H_2O_2, •OH possesses stronger oxidative power and reacts with I^- more rapidly, which may explain its closer correlation with RIS changes in response to As(V) concentrations (Fig. 7(b)). Furthermore, the correlations among components in roots under different As(V) treatments were more pronounced than those in leaves, indicating a more distinct relationship in roots.

3.4 Transcriptomic analysis and validation of the enhancement of BPF iodination mechanism in *Brassica chinensis* L. by As(V)

A transcriptomic analysis was conducted to further explore the mechanism by which As(V) enhances BPF iodination in *Brassica chinensis* L. The results showed that as As(V) concentration increased, the number of differentially expressed genes (DEGs) in the roots and leaves reached 3824 and 1618, respectively, accounting for 20.43% and 15.55% of the total DEGs in the three groups of roots and leaves (Figs. 8(a) and 8(b)). These proportions are relatively high, indicating that adding As(V) can cause significant changes and differential impacts on gene expression in *Brassica chinensis* L.

Based on the principle of prioritizing genes commonly expressed in both roots and leaves (highlighted with boxes), followed by genes regulating the same proteins (annotated with identical text), and finally genes with similar regulatory functions (indicated by the same text color), potential genes enhancing the iodination of BPF in *Brassica chinensis* L. were selected for analysis. The results showed that genes in both roots and leaves responsive to H_2O_2, ROS, and those regulating POD and SOD were predominantly upregulated to varying degrees after As(V) treatment. This further supports the proposed three pathways by which As(V) enhances the iodination of BPF in *Brassica chinensis* L.

At the same time, it can be observed that genes regulating POD in roots exhibit a stronger upregulated response to increasing As(V) concentrations compared to those in leaves. The shared gene *Bra017830* in both roots and leaves highlights this phenomenon more clearly, aligning with our PCA results (Fig. 8(c)). This further suggests that the POD pathway may be a crucial mechanism by which As(V) enhances BPF iodination in roots. Notably, since POD can couple phenoxy radicals to form coupled products (Laurenti et al., 2003; Liu et al., 2022), this further explains why at 100 μmol/L As(V), the root contains the coupled iodinated product TP7, which is absent in leaves.

Genes responsive to ROS were more strongly upregulated in leaves than in roots, as indicated by the upregulation of three shared genes *(Bra024875*, *Bra005687*, *Bra000964*). Since •OH is a type of ROS, these gene expression results further support our PCA findings and help explain why the polyhydroxylated iodinated product TP2 was present in leaves but absent in roots after As(V) treatment. Notably, genes regulating monooxygenases (such as P450 enzymes) were downregulated in roots but strongly upregulated in leaves following As(V) exposure, as observed in the shared genes *Bra008510*, *Bra020484*, and *Bra015998*. Monooxygenases, including P450 enzymes, are known for their ability to hydroxylate diphenol-like

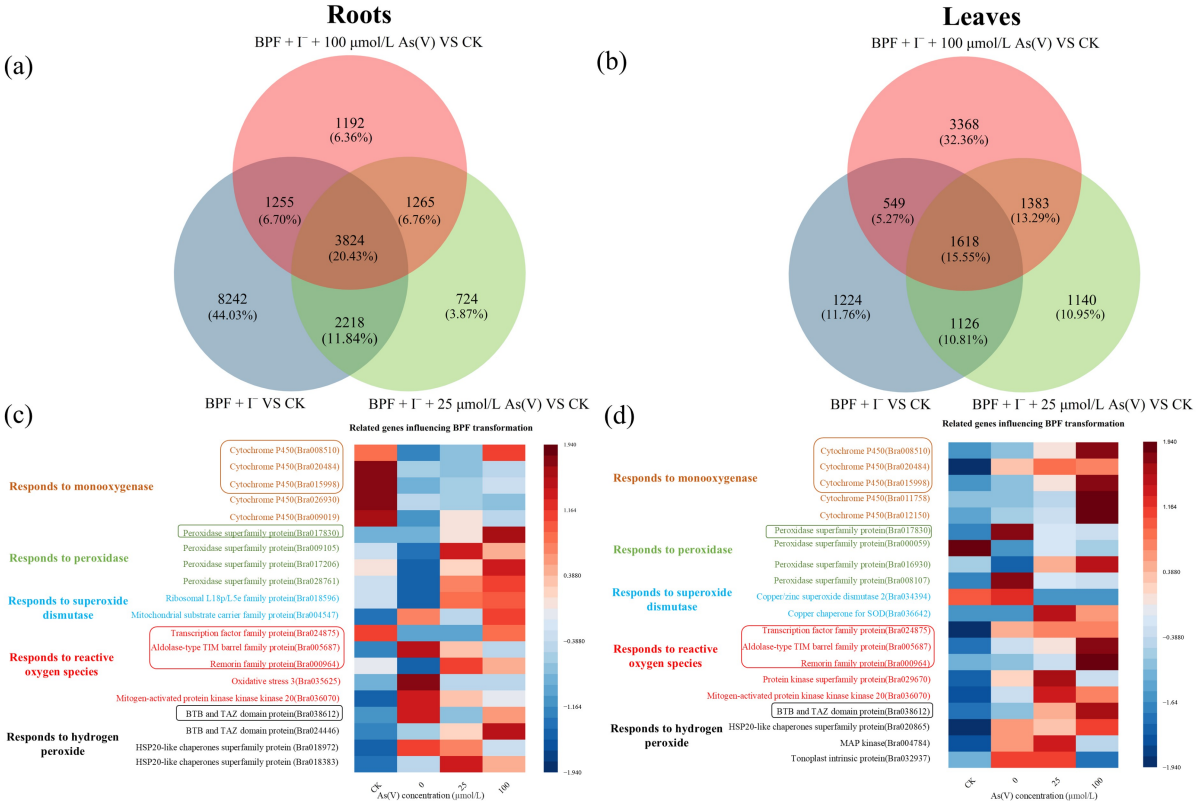

Fig. 8 The number of differentially expressed genes in roots (a) and leaves (b) in response to different As(V) treatments, and the gene expression levels in roots (c) and leaves (d) in response to RIS production pathway in different As(V) treatments.

compounds efficiently (Wang et al., 2020; Zhou and Hong, 2021), and their upregulation may also contribute to the formation of TP2 in leaves but not in roots (Fig. 8(d)).

To verify the reliability of the transcriptomic results, we selected four genes (*Bra008510*, *Bra017830*, *Bra024875*, and *Bra038612*) commonly expressed in roots and leaves, as shown in Figs. 8(c) and 8(d), for q-PCR validation. The results were almost identical to the transcriptomic findings (Fig. S15), further confirming the reliability of the transcriptomic analysis.

Based on the two analyses mentioned above, the mechanism by which As(V) enhances the iodination of BPF in *Brassica chinensis* L. likely involves three pathways: increasing POD activity, enhancing H_2O_2 content, and boosting the ability to produce •OH. POD activity and H_2O_2 content dominant roots, while the effects on •OH and H_2O_2 are more significant in leaves.

3.5 ECOSAR and T·E·S·T software toxicity evaluation of BPF iodinated products in *Brassica chinensis* L.

Seven iodinated products were analyzed for toxicity using ECOSAR and T·E·S·T software. The results revealed that TP1, TP4, TP5, TP6, and TP7 exhibited increased acute toxicity to most species. Notably, TP2 showed contradictory toxicity trends: an increase in T·E·S·T analysis and a decrease in ECOSAR analysis, likely due to differences in target species.

Whether using ECOSAR analysis or T·E·S·T analysis, the most toxic substance in the roots is TP5, which is generated after the addition of As(V) and increases with the concentration of As(V). ECOSAR analysis revealed that the toxicity of TP5 to different species increased by 2.57 to 96.30 times compared to BPF. In the T·E·S·T analysis, the toxicity also increased by 10.66 to 93.67 times. The second most toxic substance in the roots is TP7, which is produced at a concentration of 100 μmol/L. Toxicity analysis using ECOSAR and T·E·S·T found that its toxicity increased by 2.98 to 32.50 times and 7.89 to 26.30 times, respectively. In the leaves, TP1 and TP6, newly generated after the addition of As(V), showed an increase in toxicity during the ECOSAR and T·E·S·T evaluations by 1.53 to 4.85 times, 2.19 to 4.01 times, and 1.30 to 3.20 times, 1.68 to 3.01 times, respectively. These findings indicate that the iodinated products in

Brassica chinensis L. influenced by As(V) could present greater environmental hazards and potentially impact human well-being (Tables 2 and 3).

3.6 Toxicity of iodinated products extracted from different tissues of *Brassica chinensis* L. to HepG2 cells

Previous studies have indicated that bisphenol analogs exhibit cytotoxicity toward HepG2 cells (Vidyashankar et al., 2014; Geng et al., 2017; Hercog et al., 2019; Yue et al., 2019). Therefore, to further validate the toxicity of iodinated products in *Brassica chinensis* L., HepG2 cells were used for toxicity assessment in this study.

It was found that BPF levels in the different As(V) treatment groups did not cause any significant change in the viability of HepG2 cells (Figs. 9(a) and 9(b)). Similarly, lactate dehydrogenase (LDH), is a stable cytosolic enzyme rapidly released into the culture medium upon cell membrane rupture due to cell death (Horinouchi et al., 2015; Zhang et al., 2016). The activity of LDH in the cell culture medium was also not significantly altered by the changes in BPF content in roots and leaves after exposure to word self-prepared BPF solution (Figs. 9(c) and 9(d)). When As(V) was added, organic extracts from the roots resulted in a further decrease in HepG2 cell viability and an increase in LDH levels in the cell culture medium, with a significant difference in effect at 100 μmol/L. This indicates higher levels of harmful organic substances produced in the roots, a phenomenon attributed to the increased content of the iodide products TP5 and TP6 in the roots, as well as the production of TP7 at 100 μmol/L. Similarly, the organic extract from the leaves also resulted in varying decreases in cell viability and increases in LDH levels after As(V) treatment. This indicates that more types of harmful organic substances are produced in the leaves, namely the toxic iodide products TP1 and TP6 formed in the leaves when As(V) is added.

4 Conclusions

Arsenate (As(V)) significantly enhances the iodination

Table 2 The acute and chronic toxicity of bisphenol F and iodinated products to fish, daphnid, and green algae were calculated using ECOSAR software

Products	Acute toxicity (mg/L)			Chronic toxicity (mg/L)		
	Fish (LC50)	Daphnid (LC50)	Green alage (EC50)	Fish	Daphnid	Green alage
BPF	2.520	13.000	1.850	1.180	4.560	0.288
TP1	0.829	2.680	1.210	0.325	0.878	0.225
TP2	21.300	170.000	8.110	11.800	63.600	1.080
TP3	148.000	82.600	191.000	15.500	9.970	32.300
TP4	0.320	0.778	0.719	0.113	0.244	0.149
TP5	0.089	0.135	0.397	0.026	0.039	0.098
TP6	1.130	4.060	1.420	0.461	1.350	0.253
TP7	0.200	0.400	0.602	0.065	0.122	0.134

Table 3 Using T·E·S·T software to calculate the effects of BPF and its iodination products on the LC50 of Fathead minnow, the LC50 of Dephnia magna, and the IGC50 of T Pyriformis, and to make judgments on the developmental toxicity and mutagenicity of BPF and its iodide products

Products	Fathead minnow LC50 (96 h, mg/L)	Dephnia magna LC50 (48 h, mg/L)	T Pyriformis IGC50 (48 h, mg/L)	Developmental toxicity	Mutagenicity
BPF	4.29	3.64	7.89	Developmental toxicitant	mutagenicity negative
TP1	1.96	N/A	1.97	Developmental toxicitant	N/A
TP2	1.56	N/A	3.36	Developmental toxicitant	mutagenicity negative
TP3	34.80	N/A	89.25	Developmental toxicitant	mutagenicity negative
TP4	1.32	N/A	1.63	Developmental toxicitant	mutagenicity negative
TP5	4.58E-02	N/A	0.74	Developmental toxicitant	N/A
TP6	2.55	N/A	2.62	Developmental toxicitant	mutagenicity negative
TP7	7.81E-02	N/A	0.30	Developmental toxicitant	mutagenicity negative

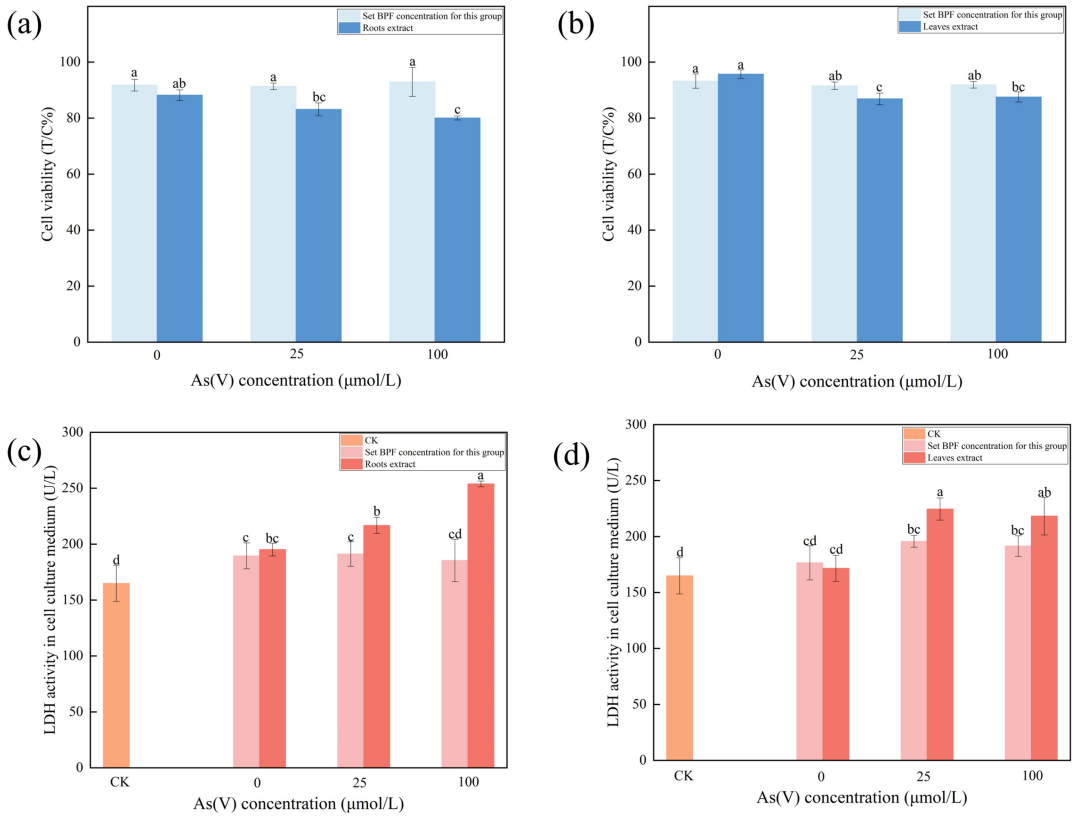

Fig. 9 Organic extracts from roots and leaves of different As(V)-treated groups (to remove the effect of inorganic ions such as As(V)) and self-configured corresponding concentrations of BPF solution (BPF concentration corresponding to 0.1 g of tissue in 1 mL system) were exposed to HepG2 cells to test the changes in cell viability (a, b) and LDH activity in their cell culture medium (c, d). The letter labeling method was used in the figure to present the results of difference analysis. Groups labeled with different letters indicate statistically significant differences ($p < 0.05$), while groups sharing the same letter indicate no significant differences.

of bisphenol F (BPF) in *Brassica chinensis* L. by inducing bursts of ROS, specifically hydrogen peroxide (H_2O_2) and hydroxyl radicals (•OH), and by increasing POD activity. H_2O_2, due to its longer lifespan, plays a crucial role in As(V)-mediated BPF iodination in roots and leaves. However, the underlying mechanisms differ: in roots, iodination is predominantly driven by elevated POD activity, whereas in leaves, it relies more on •OH bursts. Furthermore, exposure to As(V) results in the formation and accumulation of toxic iodinated byproducts, including TP5 and TP6 in roots, with the highly toxic TP7 emerging at 100 μmol/L As(V). In leaves, As(V) exposure leads to the production of additional toxic iodinated products, TP1 and TP6. These toxic compounds may be released into the soil or pore water via the root system, posing significant ecological risks. Moreover, these iodinated byproducts can enter the human body through dietary intake, directly or indirectly, potentially leading to more severe health hazards.

This study highlights the dual threat of arsenic contamination and the enhanced formation of toxic iodinated pollutants, underscoring the need for comprehensive risk assessments and mitigation strategies to protect both environmental and public health.

Conflict of Interests The authors declare that they have no known competing financial interests or personal relationships that could have appeared to influence the work reported in this paper.

Acknowledgements This study was supported by the National Key Research and Developmental Program of China (No. 2022YFC3701301), the National Natural Science Foundation of China (Nos. 42230706 and 42377428) and the Shandong Provincial Natural Science Foundation, China (Nos. ZR2020ZD34 and ZR2023YQ031), the Instrument Improvement Funds of Shandong University Public Technology Platform (China) (No. ts20230108). We thank Xiangmei Ren from Core Facilities for Life and Environmental Sciences of SKLMT (State Key Laboratory of Microbial Technology, Shandong University, China) for providing access to LC-MS/MS and technical assistance.

Electronic Supplementary Material Supplementary material is available in the online version of this article at https://doi.org/10.1007/s11783-025-2003-x and is accessible for authorized users.

References

Alam M B, Sattar M A (2000). Assessment of arsenic contamination in soils and waters in some areas of Bangladesh. Water Science and Technology, 42(7−8): 185–192

Appelo C A J, Van Der Weiden M J J, Tournassat C, Charlet L (2002). Surface complexation of ferrous iron and carbonate on ferrihydrite and the mobilization of arsenic. Environmental Science & Technology, 36(14): 3096–3103

Bednar A J, Garbarino J R, Ranville J F, Wildeman T R (2002). Preserving the distribution of inorganic arsenic species in groundwater and acid mine drainage samples. Environmental Science & Technology, 36(10): 2213–2218

Begum M C, Islam M S, Islam M, Amin R, Parvez M S, Kabir A H (2016). Biochemical and molecular responses underlying differential arsenic tolerance in rice (*Oryza sativa* L.). Plant Physiology and Biochemistry, 104: 266–277

Bhattacharjee S (2005). Reactive oxygen species and oxidative burst: roles in stress, senescence and signal transduction in plants. Current Science, 89: 1113–1121

Bianucci E, Furlan A, Tordable M D C, Hernández L E, Carpena-Ruiz R O, Castro S (2017). Antioxidant responses of peanut roots exposed to realistic groundwater doses of arsenate: identification of glutathione S-transferase as a suitable biomarker for metalloid toxicity. Chemosphere, 181: 551–561

Bichsel Y, Von Gunten U (2000). Formation of iodo-trihalomethanes during disinfection and oxidation of iodide-containing waters. Environmental Science & Technology, 34(13): 2784–2791

Brion G M, Silverstein J (1999). Iodine disinfection of a model bacteriophage, MS_2, demonstrating apparent rebound. Water Research, 33(1): 169–179

Buxton G V, Greenstock C L, Helman W P, Ross A B (1988). Critical review of rate constants for reactions of hydrated electrons, hydrogen atoms and hydroxyl radicals ($OH/\cdot O^-$ in aqueous solution). Journal of Physical and Chemical Reference Data, 17(2): 513–886

Cai D, Kong S, Shao Y, Liu J, Liu R, Wei X, Bai B, Werner D, Gao X, Li C (2022). Mobilization of arsenic from As-containing iron minerals under irrigation: effects of exogenous substances, redox condition, and intermittent flow. Journal of Hazardous Materials, 440: 129736

Chen J, Xu X, Pan X, Yao J, Li C, Qu R, Wang Z (2018). Mechanism insights into the oxidative degradation of decabromodiphenyl ethane by potassium permanganate in acidic conditions. Chemical Engineering Journal, 332: 267–276

Chen S X, Schopfer P (1999). Hydroxyl-radical production in physiological reactions. European Journal of Biochemistry, 260(3): 726–735

Chen Z, Li J, Koh K Y, Du Z, Ong C N, Chen J P (2021). Kinetics and mechanism investigation of selective arsenite oxidation by reactiveiodine species in hydrogen peroxide and iodide (H_2O_2/I^-) System. ACS ES&T Water, 1(6): 1515–1523

Claeys L, Iaccino F, Janssen C R, Van Sprang P, Verdonck F (2013). Development and validation of a quantitative structure–activity relationship for chronic narcosis to fish. Environmental Toxicology and Chemistry, 32(10): 2217–2225

Deng M, Wang S, Huang H, Ye D, Zhang X, Wang Y, Zheng Z, Liu T, Li T, Yu H (2023). Hydrogen peroxide mediates cadmium accumulation in the root of a high cadmium-accumulating rice (*Oryza sativa* L.) line. Journal of Hazardous Materials, 448: 130969

Ding G, Zhang X (2009). A picture of polar iodinated disinfection byproducts in drinking water by (UPLC/)ESI-tqMS. Environmental Science & Technology, 43(24): 9287–9293

Ding Z M, Chen Y W, Ahmad M J, Wang Y S, Yang S J, Duan Z Q, Liu M, Yang C X, Liang A X, Hua G H, et al. (2022). Bisphenol F exposure affects mouse oocyte *in vitro* maturation through inducing oxidative stress and DNA damage. Environmental Toxicology, 37(6): 1413–1422

Dodgen L K, Li J, Parker D, Gan J J (2013). Uptake and accumulation of four PPCP/EDCs in two leafy vegetables. Environmental Pollution, 182: 150–156

Dong H, Qiang Z, Richardson S D (2019). Formation of iodinated disinfection byproducts (I-DBPs) in drinking water: emerging concerns and current issues. Accounts of Chemical Research, 52(4): 896–905

Dong M, Sun N, Liu C (2023). Bromide ion enhancing the phytodegradation of emerging phenolic pollutants and its mechanisms mediating wheat resistance to phenolic pollutants stress. Journal of Cleaner Production, 411: 137295

Duan L, Wang W, Sun Y, Zhang C (2016). Iodine in groundwater of the Guanzhong Basin, China: sources and hydrogeochemical controls on its distribution. Environmental Earth Sciences, 75(11): 970

Geng S, Wang S, Zhu W, Xie C, Li X, Wu J, Zhu J, Jiang Y, Yang X, Li Y, et al. (2017). Curcumin attenuates BPA-induced insulin resistance in HepG2 cells through suppression of JNK/p38 pathways. Toxicology Letters, 272: 75–83

Glyan'Ko A K, Ischenko A A (2010). Structural and functional characteristics of plant NADPH oxidase: a review. Applied Biochemistry and Microbiology, 46(5): 463–471

Gonsioroski A, Meling D D, Gao L, Plewa M J, Flaws J A (2020). Iodoacetic acid inhibits follicle growth and alters expression of genes that regulate apoptosis, the cell cycle, estrogen receptors, and ovarian steroidogenesis in mouse ovarian follicles. Reproductive Toxicology, 91: 101–108

Gu J, Wu J, Xu S, Zhang L, Fan D, Shi L, Wang J, Ji G (2020). Bisphenol F exposure impairs neurodevelopment in zebrafish larvae (*Danio rerio*). Ecotoxicology and Environmental Safety, 188: 109870

Guo D, Wang Y, Chen C, He J, Zhu M, Chen J, Zhang C (2021). A

multi-structural carbon nitride co-modified by Co, S to dramatically enhance mineralization of Bisphenol f in the photocatalysis-PMS oxidation coupling system. Chemical Engineering Journal, 422: 130035

Hartley-Whitaker J, Ainsworth G, Meharg A A (2001). Copper- and arsenate-induced oxidative stress in Holcus anatus L. clones with differential sensitivity. Plant, Cell & Environment, 24(7): 713–722

Henriksen A, Smith A T, Gajhede M (1999). The structures of the horseradish peroxidase C-Ferulic acid complex and the ternary complex with cyanide suggest how peroxidases oxidize small phenolic substrates. Journal of Biological Chemistry, 274(49): 35005–35011

Hercog K, Maisanaba S, Filipič M, Sollner-Dolenc M, Kač L, Žegura B (2019). Genotoxic activity of bisphenol A and its analogues bisphenol S, bisphenol F and bisphenol AF and their mixtures in human hepatocellular carcinoma (HepG2) cells. Science of the Total Environment, 687: 267–276

Hetzel B S (2009). Chapter 62: iodine deficiency and the brain: an overview. In: Preedy V R, Burrow G N, Watson R, editors. Comprehensive Handbook of Iodine: Nutritional, Biochemical, Pathological, and Therapeutic Aspects. Amsterdam/Boston: Elsevier/Academic Press, 598–606

Heyno E, Mary V, Schopfer P, Krieger-Liszkay A (2011). Oxygen activation at the plasma membrane: relation between superoxide and hydroxyl radical production by isolated membranes. Planta, 234(1): 35–45

Horinouchi Y, Summers F A, Ehrenshaft M, Mason R P (2015). Free radical generation from an aniline derivative in HepG2 cells: a possible captodative effect. Free Radical Biology & Medicine, 78: 111–117

Huang T, Danaher L A, Brüschweiler B J, Kass G E N, Merten C (2019). Naturally occurring bisphenol F in plants used in traditional medicine. Archives of Toxicology, 93(6): 1485–1490

Jia J, Liu D, Wang Q, Li H, Ni J, Cui F, Tian J (2022). Comparative study on bisphenols oxidation via TiO_2 photocatalytic activation of peroxymonosulfate: effectiveness, mechanism and pathways. Journal of Hazardous Materials, 424: 127434

Johnson C (2003). The geochemistry of iodine and its application to environmental strategies for reducing the risk from iodine deficiency disorders (IDD). British Geological Survey Commissioned Report, CR/03/057N. Keyworth, Nottingham: British Geological Survey, Natural Environment Research Council

Khan I, Awan S A, Rizwan M, Ali S, Zhang X, Huang L (2021). Arsenic behavior in soil-plant system and its detoxification mechanisms in plants: a review. Environmental Pollution, 286: 117389

Khan K, Benfenati E, Roy K (2019). Consensus QSAR modeling of toxicity of pharmaceuticals to different aquatic organisms: ranking and prioritization of the DrugBank database compounds. Ecotoxicology and Environmental Safety, 168: 287–297

Kim K, Kim S H, Jeong G Y, Kim R H (2012). Relations of As concentrations among groundwater, soil, and bedrock in Chungnam, Korea: implications for As mobilization in groundwater according to the As-hosting mineral change. Journal of Hazardous Materials, 199–200: 25–35

Kovačič A, Andreasidou E, Brus A, Vehar A, Potočnik D, Hudobivnik M J, Heath D, Pintar M, Maršič N K, Ogrinc N, et al. (2023). Contaminant uptake in wastewater irrigated tomatoes. Journal of Hazardous Materials, 448: 130964

Kundu S, Biswas A, Ray A, Roy S, Das Gupta S, Ramteke M H, Kumar V, Das B K (2024). Bisphenol A contamination in Hilsa shad and assessment of potential health hazard: a pioneering investigation in the national river Ganga, India. Journal of Hazardous Materials, 461: 132532

Kushwaha B K, Singh S, Tripathi D K, Sharma S, Prasad S M, Chauhan D K, Kumar V, Singh V P (2019). New adventitious root formation and primary root biomass accumulation are regulated by nitric oxide and reactive oxygen species in rice seedlings under arsenate stress. Journal of Hazardous Materials, 361: 134–140

Laurenti E, Ghibaudi E, Ardissone S, Ferrari R P (2003). Oxidation of 2,4-dichlorophenol catalyzed by horseradish peroxidase: characterization of the reaction mechanism by UV–visible spectroscopy and mass spectrometry. Journal of Inorganic Biochemistry, 95(2): 171–176

Lehmler H J, Liu B, Gadogbe M, Bao W (2018). Exposure to bisphenol A, bisphenol F, and bisphenol S in U.S. adults and children: the national health and nutrition examination survey 2013–2014. ACS Omega, 3(6): 6523–6532

Li J, Pang S Y, Zhou Y, Sun S, Wang L, Wang Z, Gao Y, Yang Y, Jiang J (2018). Transformation of bisphenol AF and bisphenol S by manganese dioxide and effect of iodide. Water Research, 143: 47–55

Liu S, Li X, Chen B, Ouyang X, Xie Y, Chen D (2022). Phytophenol dimerization reaction: from basic rules to diastereoselectivity and beyond. Molecules, 27(15): 4842

Lu J, Wu J, Stoffella P J, Wilson P C (2013). Analysis of bisphenol A, nonylphenol, and natural estrogens in vegetables and fruits using gas ghromatography–tandem mass spectrometry. Journal of Agricultural and Food Chemistry, 61(1): 84–89

Mackeown H, Von Gunten U, Criquet J (2022). Iodide sources in the aquatic environment and its fate during oxidative water treatment: a critical review. Water Research, 217: 118417

Mascher R, Lippmann B, Holzinger S, Bergmann H (2002). Arsenate toxicity: effects on oxidative stress response molecules and enzymes in red clover plants. Plant Science, 163(5): 961–969

Matschullat J (2000). Arsenic in the geosphere: a review. Science of the Total Environment, 249(1−3): 297–312

Meharg A A, Hartley-Whitaker J (2002). Arsenic uptake and metabolism in arsenic resistant and nonresistant plant species. New Phytologist, 154(1): 29–43

Milenković M C, Stanisavljev D R (2012). Role of free radicals in modeling the iodide-peroxide reaction mechanism. Journal of Physical Chemistry A, 116(23): 5541–5548

Mishra S, Jha A B, Dubey R S (2011). Arsenite treatment induces oxidative stress, upregulates antioxidant system, and causes phytochelatin synthesis in rice seedlings. Protoplasma, 248(3): 565–577

Morales-Roque J, Carrillo-Cárdenas M, Jayanthi N, Cruz J, Pandiyan T (2009). Theoretical and experimental interpretations of phenol oxidation by the hydroxyl radical. Journal of Molecular Structure THEOCHEM, 910(1): 74–79

Nguyen S T, Nguyen H T L, Truong K D (2020). Comparative cytotoxic effects of methanol, ethanol and DMSO on human cancer cell lines. Biomedical Research and Therapy, 7(7): 3855–3859

Panda S K, Upadhyay R K, Nath S (2010). Arsenic stress in plants. Journal Agronomy & Crop Science, 196(3): 161–174

Pi K, Wang Y, Xie X, Su C, Ma T, Li J, Liu Y (2015). Hydrogeochemistry of co-occurring geogenic arsenic, fluoride and iodine in groundwater at Datong Basin, Northern China. Journal of Hazardous Materials, 300: 652–661

Porcar-Santos O, Cruz-Alcalde A, Bayarri B, Sans C (2022). Reactions of bisphenol F and bisphenol S with ozone and hydroxyl radical: kinetics and mechanisms. Science of the Total Environment, 846: 157173

Quan L J, Zhang B, Shi W W, Li H Y (2008). Hydrogen peroxide in plants: a versatile molecule of the reactive oxygen species network. Journal of Integrative Plant Biology, 50(1): 2–18

Renew S, Heyno E, Schopfer P, Liszkay A (2005). Sensitive detection and localization of hydroxyl radical production in cucumber roots and *Arabidopsis* seedlings by spin trapping electron paramagnetic resonance spectroscopy. Plant Journal, 44(2): 342–347

Richards S L, Wilkins K A, Swarbreck S M, Anderson A A, Habib N, Smith A G, Mcainsh M, Davies J M (2015). The hydroxyl radical in plants: from seed to seed. Journal of Experimental Botany, 66(1): 37–46

Shao Y, Li S, Wei X, Zhao Y, Liang J, Li X (2024). The diverse roles of halide ions in the degradation of bisphenol A via UV/peracetic acid process at different pH values: radical chemistry, and transformation pathways. Journal of Hazardous Materials, 465: 133053

Siddiqui M H, Mukherjee S, Gupta R K, Bhatt R, Kesawat M S (2024). Potassium and jasmonic acid: induced nitrogen and sulfur metabolisms improve resilience against arsenate toxicity in tomato seedlings. South African Journal of Botany, 167: 285–300

Smyth D, Johnson C C (2011). Distribution of iodine in soils of Northern Ireland. Geochemistry, 11(1): 25

Svedberg P, Inostroza P A, Gustavsson M, Kristiansson E, Spilsbury F, Backhaus T (2023). Dataset on aquatic ecotoxicity predictions of 2697 chemicals, using three quantitative structure-activity relationship platforms. Data in Brief, 51: 109719

Tang Q, Xu Q, Zhang F, Huang Y, Liu J, Wang X, Yang Y, Liu X (2013). Geochemistry of iodine-rich groundwater in the Taiyuan Basin of central Shanxi Province, North China. Journal of Geochemical Exploration, 135: 117–123

Tiwari S, Sarangi B K (2017). Comparative analysis of antioxidant response by *Pteris vittata* and *Vetiveria zizanioides* towards arsenic stress. Ecological Engineering, 100: 211–218

Tripathi R D, Srivastava S, Mishra S, Singh N, Tuli R, Gupta D K, Maathuis F J M (2007). Arsenic hazards: strategies for tolerance and remediation by plants. Trends in Biotechnology, 25(4): 158–165

Tzean Y, Wang K T, Lee P Y, Wu T M (2024). Assessing the impact of arsenite and arsenate on *Sarcodia suae*: a tale of two toxicities. Ecotoxicology, 33(8): 937–947

Vezza M E, Pramparo R D P, Wevar Oller A L, Agostini E, Talano M A (2022). Promising co-inoculation strategies to reduce arsenic toxicity in soybean. Environmental Science and Pollution Research International, 29(58): 88066–88077

Vidyashankar S, Thiyagarajan O S, Varma R S, Kumar L M S, Babu U V, Patki P S (2014). Ashwagandha (*Withania somnifera*) supercritical CO_2 extract derived withanolides mitigates bisphenol A induced mitochondrial toxicity in HepG2 cells. Toxicology Reports, 1: 1004–1012

Wagner E D, Plewa M J (2017). CHO cell cytotoxicity and genotoxicity analyses of disinfection by-products: an updated review. Journal of Environmental Sciences, 58: 64–76

Wang J, Shu Z, Chen Z, Su J, Liu C (2022a). Iodide ions enhancing sulfamerazine degradation by horseradish peroxidase/H_2O_2: degradation products, degradation mechanism and toxicity assessment. Journal of Cleaner Production, 337: 130489

Wang J, Yu P, Xie X, Wu L, Zhou M, Huan F, Jiang L, Gao R (2021a). Bisphenol F induces nonalcoholic fatty liver disease-like changes: involvement of lysosome disorder in lipid droplet deposition. Environmental Pollution, 271: 116304

Wang K, Yu H, Zhang X, Ye D, Huang H, Wang Y, Zheng Z, Li T (2022b). Hydrogen peroxide contributes to cadmium binding on root cell wall pectin of cadmium-safe rice line (*Oryza sativa* L.). Ecotoxicology and Environmental Safety, 237: 113526

Wang Q, Wen J, Zheng J, Zhao J, Qiu C, Xiao D, Mu L, Liu X (2021b). Arsenate phytotoxicity regulation by humic acid and related metabolic mechanisms. Ecotoxicology and Environmental Safety, 207: 111379

Wang W, Yu H, Qin H, Long Y, Ye J, Qu Y (2020). Bisphenol A degradation pathway and associated metabolic networks in *Escherichia coli* harboring the gene encoding CYP450. Journal of Hazardous Materials, 388: 121737

Wang Y, Li J, Ma T, Xie X, Deng Y, Gan Y (2021c). Genesis of geogenic contaminated groundwater: As, F and I. Critical Reviews in Environmental Science and Technology, 51(24): 2895–2933

Wang Y, Zheng C, Ma R (2018). Review: safe and sustainable groundwater supply in China. Hydrogeology Journal, 26(5): 1301–1324

Xu J, Wang D, Hu D, Zhang Z, Chen J, Wang Y, Zhang Y (2024). Magnetic Co-doped 1D/2D structured γ-Fe_2O_3/MoS_2 effectively activated peroxymonosulfate for efficient abatement of bisphenol A via both radical and non-radical pathways. Frontiers of

Environmental Science & Engineering, 18(3): 37

Xu L, Wong P K, Jiang Z, Yu J C (2023). Iodide-mediated selective photocatalytic treatment of phenolic pollutants. Applied Catalysis B: Environmental, 338: 123080

Yang T, Wang L, Liu Y L, Zhang W, Cheng H J, Liu M C, Ma J (2020). Ferrate oxidation of bisphenol F and removal of oxidation products with ferrate resulted particles. Chemical Engineering Journal, 383: 123167

Yao K, Zhang J, Yin J, Zhao Y, Shen J, Jiang H, Shao B (2020). Bisphenol A and its analogues in chinese total diets: contaminated levels and risk assessment. Oxidative Medicine and Cellular Longevity, 2020: 8822321

Yu H, Liu Y (2023). Impact of extended and combined exposure of bisphenol compounds on their chromosome-damaging effect—Increased potency and shifted mode of action. Environmental Science & Technology, 57(1): 498–508

Yu J, Zhu Z, Zhang H, Di G, Qiu Y, Yin D, Wang S (2020). Hydrochars from pinewood for adsorption and nonradical catalysis of bisphenols. Journal of Hazardous Materials, 385: 121548

Yue S, Yu J, Kong Y, Chen H, Mao M, Ji C, Shao S, Zhu J, Gu J, Zhao M (2019). Metabolomic modulations of HepG2 cells exposed to bisphenol analogues. Environment International, 129: 59–67

Zaborowska M, Wyszkowska J, Borowik A, Kucharski J (2023). Bisphenols—A threat to the natural Environment. Materials, 16(19): 6500

Zhang H, Wang J, Liu Y, Gong L, Sun B (2016). Wheat bran feruloyl oligosaccharides ameliorate AAPH-induced oxidative stress in HepG2 cells via Nrf2 signalling. Journal of Functional Foods, 25: 333–340

Zhou J, Hong S H (2021). Establishing efficient bisphenol A degradation by engineering *Shewanella oneidensis*. Industrial & Engineering Chemistry Research, 60(47): 16864–16873

Zhu Y G, Sun G X, Lei M, Teng M, Liu Y X, Chen N C, Wang L H, Carey A M, Deacon C, Raab A,et al. (2008). High percentage inorganic arsenic content of mining impacted and nonimpacted Chinese rice. Environmental Science & Technology, 42(13): 5008–5013